TECHNICAL ARTICLE

X-ray diffraction study of distorted perovskites $R(Co_{3/4}Ti_{1/4})O_3$ (R = La, Pr, Nd, Sm, Eu, Gd, Dy, Ho)

K. AlHamdan,[1] W. Wong-Ng,[1,a)] J. Anike,[1] and J. A. Kaduk[2]
[1]*Materials Measurement Science Division, Material Measurement Laboratory, National Institute of Standards and Technology, Gaithersburg, Maryland 20899*
[2]*Department of Chemistry, Illinois Institute of Technology, Chicago, Illinois 60616*

(Received 6 June 2017; accepted 17 August 2017)

The crystal structure and powder patterns were prepared for the distorted perovskite series $R(Co_{3/4}Ti_{1/4})O_3$ (R = La, Pr, Nd, Sm, Eu, Gd, Dy, Ho). The $R(Co_{3/4}Ti_{1/4})O_3$ members are isostructural with each other and are crystallized in the orthorhombic crystal system with space group *Pnma*, $Z = 4$. From R = La to Ho, the lattice parameters a range from 5.4614(3) to 5.5368(2) Å, b range from 7.7442(4) to 7.4859(2) Å, and c range from 5.5046(3) to 5.2170(2) Å. The unit-cell volumes, V which range from 232.81(2) to 216.237(11) Å^3 follow the trend of "lanthanide contraction". The structure distortion of these compounds is evidenced in the tilt angles θ, ϕ, and ω, which represent rotations of an octahedron about the pseudo-cubic perovskite $[110]_p$, $[001]_p$ and $[111]_p$ axes. All three tilt angles increase across the lanthanide series (for R = La to R = Ho: θ increases from 8.34° to 17.00°, ϕ from 6.24° to 8.53°, and ω from 10.41° to 18.96°), indicating a greater octahedral distortion as the ionic radius of R^{3+} [$r(R^{3+})$] decreases. The bond valence sum values for the (Co/Ti) site and the R site of $R(Co_{3/4}Ti_{1/4})O_3$ reveal no significant bond strain in these compounds. X-ray diffraction patterns of the $R(Co_{3/4}Ti_{1/4})O_3$ samples were submitted to the Powder Diffraction File. © *2017 International Centre for Diffraction Data*. [doi:10.1017/S0885715617001014]

Key words: $R(Co_{3/4}Ti_{1/4})O_3$ (R = La, Pr, Nd, Sm, Eu, Gd, Dy, Ho), crystal structure, X-ray powder diffraction patterns

I. INTRODUCTION

The continuing demand for environmentally friendly alternative energy technologies has led to increased activities in the area of thermoelectric research. For high-temperature waste heat conversion applications, low-dimensional layered oxides, in both thin film and bulk forms, have been found to have relatively high efficiency (Tritt, 1996; Ghamaty and Eisner, 1999; Venkatasubramanian *et al.*, 2001; Hsu *et al.*, 2004; Dresselhaus *et al.*, 2007). The efficiency and performance of thermoelectric energy conversion or cooling is related to the dimensionless figure of merit (ZT) of the thermoelectric (TE) materials, given by $ZT = S^2T/\rho\kappa$, where T is the absolute temperature, S is the Seebeck coefficient or thermoelectric power, ρ is the electrical resistivity, and κ is the thermal conductivity (Nolas *et al.*, 2001).

The search for oxide compounds with superior thermoelectric properties, including perovskites, continues. Examples of these oxides include $La_{1-x}A_xCoO_3$ (A = Pb, Na) (He *et al.*, 2006), $NaCoO_x$ (Terasaki *et al.*, 1997), $Ca_2Co_3O_6$ (Mikami *et al.*, 2003; Mikami and Funahashi, 2005), $Ca_3Co_4O_9$ (Masset *et al.*, 2000; Mikami *et al.*, 2002; Grebille *et al.*, 2004; Hu *et al.*, 2005), $Bi_2Sr_2Co_2O_x$ (Shin and Murayama, 2000; Wang *et al.*, 2009), $Ba_2Ho(Cu_{3-x}Co_x)O_{6+x}$ (Wong-Ng *et al.*, 2002), and (Bi,Pb)CuSeO (Hiramatsu *et al.*, 2008; Luu and Vaquelro, 2013; Wong-Ng, *et al.*, 2016a). Phase diagram and structure/property relationship research using CaO and Co_3O_4 as two of the end members have been reported (Wong-Ng *et al.*, 2010, 2011, 2013, 2014). $R(Co_{3/4}Ti_{1/4})O_3$ is a series of distorted pervoskite materials that may have potential for thermoelectric applications.

Since X-ray diffraction (XRD) is a non-destructive technique for phase identification, XRD patterns are especially important for phase characterization. The main goal of this investigation is to determine and compare the crystal structure and crystal chemistry for $R(Co_{3/4}Ti_{1/4})O_3$ (R = La, Pr, Nd, Sm, Eu, Gd, Dy, Ho, Er, Tm, Yb, and Lu). The second goal is to determine the experimental patterns and to make these patterns broadly available through submission to the Powder Diffraction File (PDF) (Wong-Ng *et al.*, 2001; PDF, 2017).

II. EXPERIMENTAL DETAILS

A. Sample preparation

The $R(Co_{3/4}Ti_{1/4})O_3$ samples were prepared from stoichiometric amounts of R_2O_3 (R = La, Pr, Nd, Sm, Eu, Gd, Dy, Ho, Er, Tm, Yb and Lu), Co_3O_4, and TiO_2 using solid-state high-temperature techniques. The starting samples were mixed, pelletized, and heat treated in air at 750 °C for 1 day and subsequently at 850 °C for 4 days, 1000 °C for 5 days, 1025 °C for 60 h. These samples except for R = La, Pr, and Nd were further heat treated at 1075 °C for 108 h. Samples with smaller ionic radius of R^{3+} such as those with R = Er, Tm, and Yb were heat treated further at 1075 °C for another

a)Author to whom correspondence should be addressed. Electronic mail: winnie.wong-ng@nist.gov

160 h, and at 1250 °C for 60 h. During each heat treatment, the samples were furnace cooled. The heat treatment process was repeated until no further changes were detected in the powder XRD patterns.

B. X-ray Rietveld refinements and powder reference patterns

The $R(Co_{3/4}Ti_{1/4})O_3$ powders were mounted on quartz zero-background cells. The powder patterns were measured from 5 to 130° in 0.020 214 4° steps using Cu$K\alpha$ radiation on a Bruker D2 Phaser diffractometer equipped with a LynxEye detector. NIST SRM 660a LaB_6 was used as external calibration standard. The Rietveld refinement technique (Rietveld, 1969) with the software suites EXPGUI (Toby, 2001) and GSAS (Larson and von Dreele, 2004) was used to determine the structure of $R(Co_{3/4}Ti_{1/4})O_3$. All Co/Ti sites were refined assuming 3:1 occupancy.

The constant wavelength Pseudo-Voigt profile function (function #2 with 18 terms) was used for all refinements (Howard, 1982; Thompson *et al.*, 1987); only the LY and specimen displacement coefficients were refined. GSAS offers a number of different background functions. For each of these functions, the number of terms to be used is adjustable. The larger the number of terms, the more complex the shape that can be fit. In theory, each function will have advantages under different circumstances. In general, the Shifted Chebyschev (type #1) is preferable to the others for the vast majority of Rietveld refinements. In this work, background correction was performed using the GSAS background function #1 with six terms, and an absorption/surface roughness correction was applied using function #3.

Reference patterns were obtained with a Rietveld pattern decomposition technique. Using this technique, the reported peak intensities were derived from the extracted integrated intensities, and positions calculated from the lattice parameters. When peaks are not resolved at the resolution function, the intensities are summed, and an intensity-weighted d-spacing is reported. They are also corrected for systematic errors both in d-spacing and intensity. In summary, these patterns represent ideal specimen patterns.

C. Bond valence sum (BVS) (V_b) calculations

The BVS values, V_b, for R, Co, and Ti were calculated using the Brown–Altermatt empirical expression (Brown and Altermatt, 1985; Brese and O'Keeffe, 1991), and the results are also listed in Table III. The V_b of an atom i is defined as the sum of the bond valences v_{ij} of all the bonds from atoms i to atoms j. The most commonly adopted empirical expression for the bond valence v_{ij} as a function of the interatomic distance d_{ij} is $v_{ij} = \exp[(R_0 - d_{ij})/B]$. The parameter, B, is commonly taken to be an "universal" constant equal to 0.37 Å. The values for the R_0 reference distances are, R_0 are: Ti^{3+}–O 1.791, Co^{3+}–O 1.70; La^{3+}–O 2.172; Pr^{3+}–O 2.135, Nd^{3+}–O 2.117, Sm^{3+}–O 2.088, Eu^{3+}–O 2.076, Gd^{3+}–O 2.065, Dy^{3+}–O 2.036, Ho^{3+}–O 2.023, Er^{3+}–O 2.010, Tm^{3+}–O 2.000, Yb^{3+}–O 1.985, and Lu^{3+}–O 1.971. For sites shared by more than one species, the resulting BVS is the weighted sum using the site occupancies.

III. RESULTS AND DISCUSSION

Among the 12 $R(Co_{3/4}Ti_{1/4})O_3$ samples that we prepared, only eight of them which have relatively larger size of R form single phase, namely, with R = La, Pr, Nd, Sm, Eu, Gd, Dy, Ho. Single phases were not formed for the compositions with R = Er, Tm, and Yb. Figure 1 gives the results of Rietveld refinements for $Nd(Co_{3/4}Ti_{1/4})O_3$, as an example. It is a least-squares plot to highlight the weak reflections (Larson and von Dreele,

TABLE I. Rietveld refinement residuals for $R(Co_{3/4}Ti_{1/4})O_3$ (R = La, Pr, Nd, Sm, Eu, Gd, Dy, Ho).

R	R_{wp}	R_p	χ^2	#Parameters
La	0.0795	0.0626	0.96	22
Pr	0.0766	0.0592	0.88	22
Nd	0.0761	0.0591	0.84	22
Sm	0.0536	0.0421	0.90	22
Eu	0.0522	0.0413	0.90	22
Gd	0.0541	0.0419	1.05	22
Dy	0.0588	0.0462	0.86	22
Ho	0.0600	0.0477	0.88	23

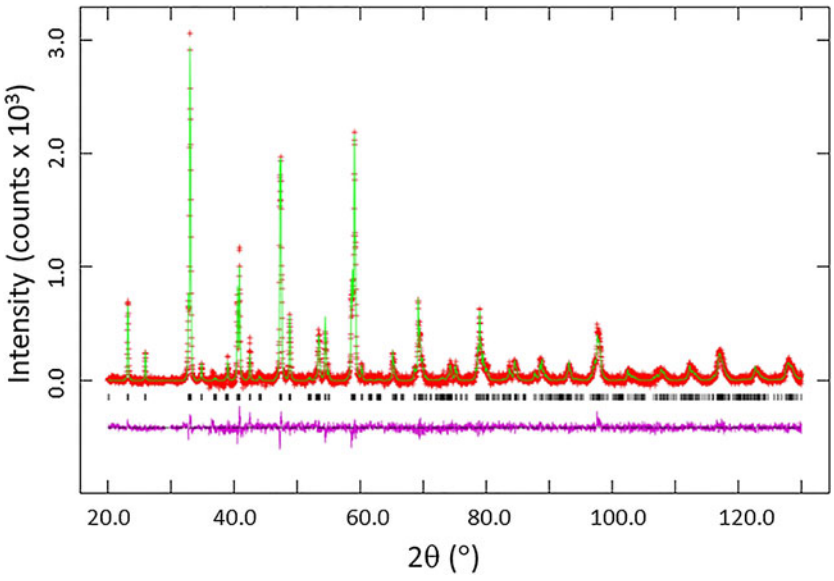

Figure 1. (Color online) Observed (crosses), calculated (solid line), and difference XRD pattern (bottom) for Nd $(Co_{3/4}Ti_{1/4})O_3$ by Rietveld analysis technique. The difference pattern is plotted at the same scale as the other calculated peak positions. For $2\theta > 36°$, the vertical scale has been multipled by a factor of 3.

TABLE II. Cell parameters for $R(Co_{3/4}Ti_{1/4})O_3$ (R = La, Pr, Nd, Sm, Eu, Gd, Dy, Ho); orthorhombic, *Pnma*, $Z = 4$ [uncertainties refer to standard deviation; $r(R^{3+})$ (Å) is the ionic radius for R(VIII coordination) for R = Pr, Nd, Sm, Eu, Gd, Dy, Ho, and R(IX) for R = La].

Chemical formula	a (Å)	b (Å)	c (Å)	V (Å^3)	d_{cal}	$r(R^{3+})$(Å)
$La(Co_{3/4}Ti_{1/4})O_3$	5.4614 (3)	7.7442 (4)	5.5046 (3)	232.81 (2)	6.935	1.216
$Pr(Co_{3/4}Ti_{1/4})O_3$	5.462 18 (12)	7.6886 (2)	5.435 02 (13)	228.252 (9)	7.132	1.126
$Nd(Co_{3/4}Ti_{1/4})O_3$	5.466 41 (13)	7.6606 (2)	5.403 54 (14)	226.278 (12)	7.292	1.109
$Sm(Co_{3/4}Ti_{1/4})O_3$	5.5083 (2)	7.6114 (2)	5.3493 (2)	224.231 (14)	7.540	1.079
$Eu(Co_{3/4}Ti_{1/4})O_3$	5.5220 (2)	7.5834 (3)	5.3192 (2)	222.745 (14)	7.638	1.066
$Gd(Co_{3/4}Ti_{1/4})O_3$	5.5369 (4)	7.5583 (5)	5.2906 (4)	221.41 (4)	7.842	1.053
$Dy(Co_{3/4}Ti_{1/4})O_3$	5.5336 (2)	7.5008 (4)	5.2374 (2)	217.39 (2)	8.148	1.027
$Ho(Co_{3/4}Ti_{1/4})O_3$	5.5368 (2)	7.4859 (2)	5.2170 (2)	216.237 (11)	8.266	1.015

2004), where observed (crosses), calculated (solid line), and difference XRD patterns (bottom) are shown. The tick marks indicate the calculated peak positions, and the difference pattern is plotted on the same scale as other patterns. For $2\theta > 36°$, the vertical scale has been multiplied by a factor of 3.

Table I gives the refinement results for $R(Co_{3/4}Ti_{1/4})O_3$. Table II reports the lattice parameters and calculated density D_x. As expected, the D_x values increase as the size of ionic radius, $r(R^{3+})$ (Shannon, 1976) decreases. The atomic coordinates and displacement parameters are given in Table III. Tables IV–VII summarize the bond distances, selected bond angles, tilt angles, and BVS values. It is seen from Table VI that the Co/Ti sites are all sixfold coordinated, having a distorted octahedral environment. The coordination number (C.N.) for R–O is 8 for all compounds except for La–O which is 9 (with R^{3+}–O bond distances <3 Å).

TABLE III. Atomic coordinates and displacement factors for compounds for $R(Co_{3/4}Ti_{1/4})O_3$ (R = La, Pr, Nd, Sm, Eu, Gd, Dy, and Ho).

Atom	x	y	z	Site occupancy	U_{iso}	Wyckoff symbol
(1) $La(Co_{3/4}Ti_{1/4})O_3$						
La1	0.0184(4)	0.25	−0.0041(11)	1.0	0.0190(4)	4c
Ti2/Co3	0.0	0.0	0.5	0.25/0.75	0.0147(6)	4a
O4	0.4946(6)	0.25	0.0513(13)	1.0	0.026(2)	4c
O5	0.2775(12)	0.0258(7)	0.7228(12)	1.0	0.026(2)	8d
(2) $Pr(Co_{3/4}Ti_{1/4})O_3$						
Pr1	0.0363(2)	0.25	−0.0055(8)	1.0	0.0167(3)	4c
Ti2/Co3	0.0	0.0	0.5	0.25/0.75	0.0103(6)	4a
O4	0.4908(6)	0.25	0.0681(10)	1.0	0.021(2)	4c
O5	0.2837(9)	0.0342(5)	0.7158(9)	1.0	0.021(2)	8d
(3) $Nd(Co_{3/4}Ti_{1/4})O_3$						
Nd1	0.0424(2)	0.25	−0.0058(8)	1.0	0.0164(4)	4c
Ti2/Co3	0.0	0.0	0.5	0.25/0.75	0.0117(7)	4a
O4	0.482(2)	0.25	0.083(4)	1.0	0.013(3)	4c
O5	0.293(2)	0.042 (2)	0.712(3)	1.0	0.013(3)	8d
(4) $Sm(Co_{3/4}Ti_{1/4})O_3$						
Sm1	0.0538(2)	0.25	−0.0127(5)	1.0	0.0169(4)	4c
Ti2/Co3	0.0	0.0	0.5	0.25/0.75	0.0130(8)	4a
O4	0.4878(6)	0.25	0.0843(8)	1.0	0.034(3)	4c
O5	0.2834(8)	0.0421(4)	0.7146(9)	1.0	0.034(3)	8d
(5) $Eu(Co_{3/4}Ti_{1/4})O_3$						
Eu1	0.0588(2)	0.25	−0.0133(5)	1.0	0.0164(5)	4c
Ti2/Co3	0.0	0.0	0.5	0.25/0.75	0.0100(8)	4a
O4	0.4868(6)	0.25	0.0902(7)	1.0	0.034(3)	4c
O5	0.2832(8)	0.0449(4)	0.7143(9)	1.0	0.028(3)	8d
(6) $Gd(Co_{3/4}Ti_{1/4})O_3$						
Gd1	0.0629(3)	0.25	−0.0152(6)	1.0	0.0186(6)	4c
Ti2/Co3	0.0	0.0	0.5	0.25/0.75	0.0148(11)	4a
O4	0.4853(7)	0.25	0.0948(8)	1.0	0.022(3)	4c
O5	0.2829(9)	0.0471(5)	0.7140(10)	1.0	0.022(3)	8d
(7) $Dy(Co_{3/4}Ti_{1/4})O_3$						
Dy1	0.0678(2)	0.25	−0.0176(5)	1.0	0.0169(6)	4c
Ti2/Co3	0.0	0.0	0.5	0.25/0.75	0.0131(11)	4a
O4	0.4853(6)	0.25	0.1071(7)	1.0	0.024(4)	4c
O5	0.2814(8)	0.0531(4)	0.7151(9)	1.0	0.024(4)	8d
(8) $Ho(Co_{3/4}Ti_{1/4})O_3$						
Ho1	0.0699(2)	0.25	−0.0206(4)	1.0	0.0214(6)	4c
Ti2/Co3	0.0	0.0	0.5	0.25/0.75	0.0152(9)	4a
O4	0.4832(6)	0.25	0.1082(6)	1.0	0.040(3)	4c
O5	0.2854(7)	0.0535(4)	0.7103(8)	1.0	0.040(3)	8d

TABLE IV. Bond distances (Å) (<3 Å) for $R(Co_{3/4}Ti_{1/4})O_3$ (R = La, Pr, Nd, Sm, Eu, Gd, Dy, Ho).

Atom	Atom	Distances (Å)							
		La	Pr	Nd	Sm	Eu	Gd	Dy	Ho
R	O4	2.496(10)	2.390(7)	2.31(2)	2.320(5)	2.285(5)	2.410(4)	2.400(4)	2.385(10)
	O4	2.618(4)	2.515(4)	2.448(13)	2.446(4)	2.427(4)	2.265(6)	2.198(5)	2.204(4)
	O4	2.877(4)							
	O5	2.489(6) ×2	2.442(4) ×2	2.373(11) ×2	2.427(4) ×2	2.424(4) ×2	2.410(4) ×2	2.353(7) ×2	2.358(6) ×2
	O5	2.698(4) ×2	2.622(7) ×2	2.60(2) ×2	2.496(7) ×2	2.460(6) ×2	2.427(8) ×2	2.401(4) ×2	2.372(4) ×2
	O5	2.714(9) ×2	2.681(7) ×2	2.68(2) ×2	2.688(6) ×2	2.689(6) ×2	2.691(6) ×2	2.711(5) ×2	2.693(5) ×2
Co/Ti	O4	1.9567(11) ×2	1.9581(10) ×2	1.970(5) ×2	1.9567(10) ×2	1. 948(3) ×2	1.9567(11) ×2	1.9589(10) ×2	1.9570(9) ×2
	O5	1.9597(12) ×2	1.9613(11) ×2	1.951(15) ×2	1.9639(11) ×2	2.002(4) ×2	1.9650(12) ×2	1.9620(10) ×2	1.9638(10) ×2
	O5	1.9609(12) ×2	1.9623(11) ×2	1.996(14) ×2	1.9639(11) ×2	1.984(4) ×2	1.9650(12) ×2	1.9626(10) x2	1.9650(10) x2

TABLE V. Bond angles M–O4–M (°) and M–O5–M (°) for $R(Co_{3/4}Ti_{1/4})O_3$ (R = La, Pr, Nd, Sm, Eu, Gd, Dy, Ho) (M represents mixed (Co/Ti) sites).

M	La	Pr	Nd	Sm	Eu	Gd	Dy	Ho
M–O4–M	163.3(4)	158.0(3)	158.0(3)	153.0(2)	151.3(2)	149.9(3)	146.4(2)	146.0(2)
M–O5–M	162.9(3)	158.8(2)	158.2(2)	155.6(2)	154.7(2)	154.0(2)	152.2(2)	151.0(2)

TABLE VI. Estimated tilt angles θ, ϕ, and ω (°) for $R(Co_{3/4}Ti_{1/4})O_3$ (R = La, Pr, Nd, Sm, Eu, Gd, Dy, Ho).

Site	La	Pr	Nd	Sm	Eu	Gd	Dy	Ho
θ	8.34	11.00	13.48	13.47	14.36	15.05	16.82	17.00
ϕ	6.24	7.73	9.23	7.83	7.84	7.84	7.54	8.53
ω	10.41	13.42	16.29	15.55	16.32	16.93	18.39	18.96

TABLE VII. Bond valence sum (BVS) for $R(Co_{3/4}Ti_{1/4})O_3$ (R = La, Pr, Nd, Sm, Eu, Gd, Dy, Ho) (if more than one atom types occupy the same site, the resulting BVS is the weighted sum of each site occupancy; the ideal BVS values are 3.0 for the R–O site and 3.0 for the Co/Ti–O site, respectively).

Site	La	Pr	Nd	Sm	Eu	Gd	Dy	Ho
R	2.659	2.726	2.982	2.773	2.826	2.883	2.937	2.904
Co/Ti	3.184	3.171	3.076	3.163	3.031	3.157	3.166	3.160

$R(Co_{3/4}Ti_{1/4})O_3$ phases adopt the orthorhombic *Pnma* (#62) symmetry, as determined by the combined anti-phase and in-phase octahedral rotations, which can be described as $a^-a^-c^+$ using Glazer's notation (Glazer, 1972). The unit-cell volume (Figure 2) for $R(Co_{3/4}Ti_{1/4})O_3$ decreases monotonically with the decreasing size of $r(R^{3+})$, from La to Ho, respectively. The volume decrease is mainly because of the smaller b and c lattice parameters, although the magnitude of the a-parameter maintains an opposite trend (Table II). This trend implies that the twisting of the [(Ti/Co)O_6] octahedra in $R(Co_{3/4}Ti_{1/4})O_3$ has a larger influence on the magnitude of the a cell parameter, while that of the size of polyhedra, [RO_x], has a stronger effect on b and c.

Figures 3 and 4 illustrate the structure of $R(Co_{3/4}Ti_{1/4})O_3$. In orthorhombic $R_2M_2O_6$ ("M" is used to represent the mixed site Co/Ti), there are two distinct M–O–M angles (M–O4–M and M–O5–M) that relate neighboring octahedra. The M–O4–M angle (Figure 3) and the M–O5–M angles (Figure 4) which both deviate from the ideal value of 180° reflect the degree of octahedral tilting. For example, from R = La to Ho, the O4–M–O4 angle decreases from 163.3(4) to 146.0 (2)°, and the M–O5–M angle decreases from 162.9(3) to 151.0(2)°, respectively. The three tilt angles θ, ϕ, and ω that follow the notation of Zhao *et al.* (1993a, 1993b) to represent rotations of octahedral about the pseudo-cubic $[110]_p$, $[001]_p$, and $[111]_p$ axes, respectively, are shown in Table V (Figure 5). All the three tilt angles increase from R = La to R = Ho: θ from 8.34 to 17.00°, ϕ from 6.24 to 8.53°, and ω from 10.41 to 18.96°, respectively. This increase across the lanthanide series indicates a greater octahedral distortion as the size of R^{3+} decreases.

The Goldschmidt geometrical tolerance factor (t) is a criterion for the stability and distortion of perovskite structures, ABO_3. It can also be used to calculate the compatibility of an ion with a crystal structure. The tolerance factor t is defined as $t = <r_A + r_O>/\sqrt{2}<r_B + r_O>$ (Goldschmidt, 1926), where r_A, r_B, and r_O represent the ionic radii of A-cations, B-cations, and oxygen, respectively. In the ideal cubic structure with $t = 1$, the unit-cell parameter a can be described as $a = \sqrt{2}<r_A + r_O> = 2<r_B + r_O>$. As t approaches 1, the structure is expected to become less distorted; with $t < 1$ the distortion is accommodated by the cooperative rotations of the [BO_6] octahedra, resulting in a lower symmetry. In $R(Co_{3/4}Ti_{1/4})O_3$, the C.N. ranges from 8 to 9 for R^{3+} sites and 6 for the Co^{3+}/Ti^{3+}

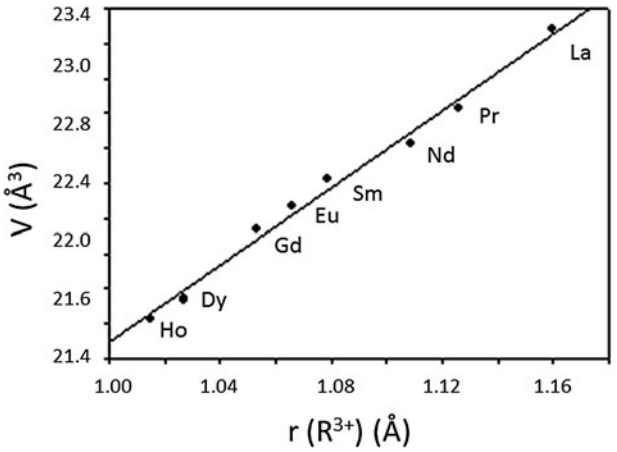

Figure 2. Plot of unit-cell volume, V, of $R(Co_{3/4}Ti_{1/4})O_3$ (R = La, Pr, Nd, Sm, Eu, Gd, Dy, Ho) vs. ionic radius. A monotonic decrease of V is observed.

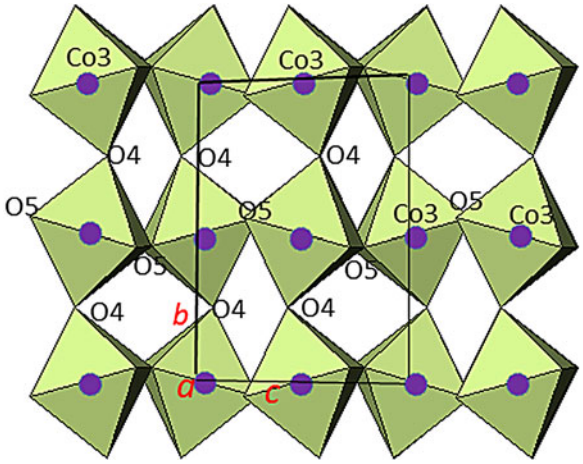

Figure 3. (Color online) Crystal structure of $R(Co_{3/4}Ti_{1/4})O_3$ based on X-ray powder data (viewed along the a-axis), showing the labeling of selected atoms, and the coordination environments of the cation sites (M refers to the mixed Co/Ti sites).

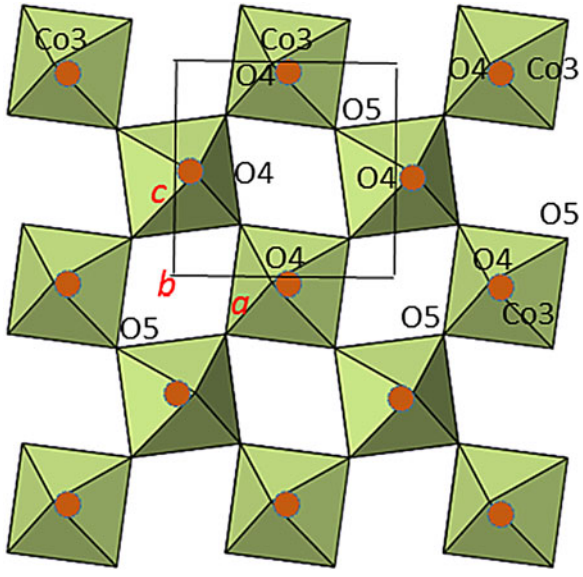

Figure 4. (Color online) Crystal structure of $R(Co_{3/4}Ti_{1/4})O_3$ based on X-ray powder data viewed along the b-axis, showing the labeling of selected atoms, and the coordination environments of the cation sites (M refers to the mixed Co/Ti sites).

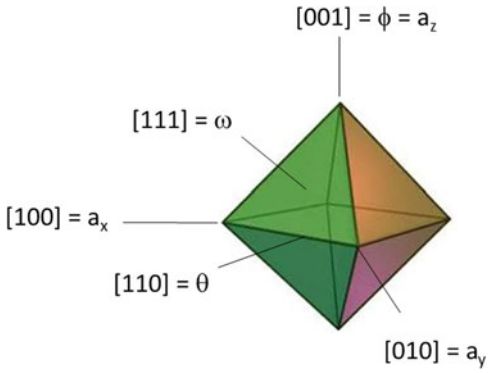

Figure 5. (Color online) The three tilt angles θ, ϕ, and ω which follow the notation of Zhao *et al.* (1993a, 1993b) represent rotations of the MO_6 octahedron about the pseudo-cubic $[110]_p$, $[001]_p$, and $[111]_p$ axes, respectively, where M stands for Co/Ti.

sites. The experimental R–O and Co/Ti–O values are used to compute the t values. As $r(R^{3+})$ decreases across the lanthanide series, so do the t values. The t values for $R(Co_{3/4}Ti_{1/4})O_3$, as R = La, Pr, Nd, Sm, Eu, Gd, Dy, and Ho are 0.913, 0.882, 0.876, 0.866, 0.861, 0.857, 0.848, and 0.843, respectively. Most of these t values (from R = Pr to R = Ho) fall in the range of Goldschmidt "orthorhombic/rhombohedral" structure type, approximately 0.71–0.90 (Goldschmidt, 1926), except for the R = La compound that shows the structure type to be orthorhombic, but with a small tendency to be cubic. The trends of both the tilt angles and the Goldschmidt geometrical tolerance factor (t) are similar to that of the series of $R(Co_{0.5}\ Fe_{0.5})O_3$ (R = Pr, Nd, Sm, Eu, Gd) (Wong-Ng *et al.*, 2016b), which also has a similar distorted pervoskite structure.

The BVS values (Table VII) for the R^{3+} sites in $R(Co_{3/4}Ti_{1/4})O_3$ were found to range from 2.659 to 2.988, indicating somewhat underbonding situation (oversized cages where R^{3+} reside, as the BVS values are less than the ideal value of 3.0); whereas for the (Co/Ti)–O sites, the VBS values range from 3.031 to 3.166, indicating slightly overbonding situation (cage too small).

IV. REFERENCE XRD PATTERNS

An example of the reference patterns of the $Nd(Co_{3/4}Ti_{1/4})O_3$ phase is given in Table VIII. In this pattern, the symbols "*M*" and "+" refer to peaks containing contributions from two and more than two reflections, respectively. The peak that has the strongest intensity in the entire pattern is assigned an intensity of 999 and other lines are scaled relative to this value. In general, the d-spacing values are calculated values from refined lattice parameters. The intensity values reported are integrated intensities (rather than peak heights) based on the corresponding profile parameters. For resolved overlapped peaks, intensity-weighted calculated d-spacing, along with the observed integrated intensity and the hkl indices of both peaks (for "*M*"), or the hkl indices of the strongest peak (for "+") are used. For peaks that are not resolved at the instrumental resolution, the intensity-weighted average d-spacing and the summed integrated intensity value are used. In the case of a cluster, unconstrained profile fits often reveal the presence of multiple peaks, even when they are closer than the instrumental resolution. In this situation, both d-spacing and

TABLE VIII. X-ray powder pattern for $Nd(Co_{3/4}Ti_{1/4})O_3$ (*Pnma*, $Z = 4$), $a = 5.466\,41(13)$ Å, $b = 7.6606(2)$ Å, $c = 5.403\,54(14)$ Å, $V = 226.278(12)$ Å^3, $D_x = 7.29$ g cm^{-3}) (the symbol "*M*" refers to peaks containing contributions from two reflections; the particular peak that has the strongest intensity in the entire pattern is assigned an intensity of 999 and other lines are scaled relative to this value; the *d*-spacing values are calculated values from refined lattice parameters, and "*I*" represents integrated intensity values).

d_{cal}	I_{obs}	*h*	*k*	*l*	d_{cal}	I_{obs}	*h*	*K*	*l*	d_{cal}	I_{obs}	*h*	*k*	*l*
3.8384	262	1	0	1*M*	3.8384	262	0	2	0*M*	3.4349	54	1	1	1
2.7332	225	2	0	0	2.7129	999	1	2	1	2.7018	245	0	0	2
2.5743	61	2	1	0	2.3092	14	1	1	2*M*	2.3092	14	0	3	1*M*
2.2249	93	2	2	0	2.2078	132	0	2	2	2.1268	48	1	3	1
2.0573	13	2	2	1	1.9215	254	2	0	2	1.9152	160	0	4	0
1.8645	99	2	3	0*M*	1.8645	9	2	1	2*M*	1.7175	28	2	2	2
1.7141	44	1	4	1	1.7107	24	1	0	3	1.6844	80	3	1	1
1.6696	11	1	1	3	1.5741	124	3	2	1	1.5684	93	2	4	0
1.5621	337	0	4	2*M*	1.5621	337	1	2	3*M*	1.5353	21	2	3	2
1.4303	50	3	3	1	1.3666	15	4	0	0	1.3564	132	2	4	2
1.3509	39	0	0	4	1.3454	25	4	1	0	1.2768	7	0	6	0
1.2758	19	1	4	3	1.2740	7	0	2	4	1.2634	26	3	1	3
1.2195	18	4	0	2	1.2148	49	3	2	3	1.2115	111	1	6	1*M*
1.2115	111	2	0	4*M*	1.2045	42	4	3	0*M*	1.2045	42	4	1	2*M*
1.1979	16	2	5	2	1.1962	13	2	1	4	1.1545	24	2	2	4*M*
1.1545	24	0	6	2*M*	1.1460	27	3	5	1	1.1450	26	3	3	3
1.1413	7	1	5	3	1.1124	21	4	4	0	1.1039	41	0	4	4
1.1004	32	4	3	2	1.0942	12	2	3	4	1.0634	10	2	6	2
1.0612	31	5	1	1	1.0602	7	1	0	5	1.0286	22	4	4	2
1.0266	30	3	6	1	1.0234	103	2	4	4*M*	1.0234	103	1	6	3*M*
1.0218	62	1	2	5	1.0199	16	4	5	0	0.9981	29	5	3	1
0.9827	12	3	5	3	0.9576	13	0	8	0	0.9541	14	4	5	2
0.9533	20	4	1	4	0.9510	5	2	7	2	0.9501	5	2	5	4
0.9277	41	5	1	3*M*	0.9277	41	1	4	5*M*	0.9243	14	3	7	1
0.9228	14	3	1	5	0.9080	10	5	2	3	0.9047	12	6	1	0
0.9043	32	3	6	3	0.9037	26	2	8	0	0.9033	41	3	2	5
0.9026	31	0	8	2	0.9006	11	0	0	6	0.8991	19	4	3	4
0.8781	26	5	5	1	0.8777	24	5	3	3	0.8735	10	3	3	5
0.8587	20	4	4	4	0.8580	45	6	3	0*M*	0.8580	45	6	1	2*M*
0.8570	42	2	8	2	0.8554	19	2	0	6					

intensity values are reported independently. All patterns have been submitted for inclusion in the PDF.

V. SUMMARY

Crystal structure and X-ray powder reference patterns of $R(Co_{3/4}Ti_{1/4})O_3$ (R = La, Pr, Nd, Sm, Eu, Gd, Dy, Ho) series of compounds have been determined. $R(Co_{3/4}Ti_{1/4})O_3$ belongs to the distorted perovskite structure type, with a space group of *Pnma*, $Z = 4$. We have characterized and compared the structure including the degrees of distortion across the series using the tilt angles θ, ϕ, and ω. The Goldsmidth tilt angle calculations ("*t*" decreases from 0.913 to 0.843 for compounds of R = La to Ho) indicate the structure to be of the "orthorhombic/rhombohedral" structure type, except for the R = La compound, which also has a small tendency to be cubic. The powder patterns of the $R(Co_{3/4}Ti_{1/4})O_3$ series have been submitted to the PDF.

ACKNOWLEDGEMENT

ICDD is acknowledged for the Grant-in-Aid assistance for the project.

Brese, N. E. and O'Keeffe, M. (**1991**). "Bond-valence parameters for solids," Acta Crystallogr. B **47**, 192–197.

Brown, I. D. and Altermatt, D. (**1985**). "Bond-valence parameters obtained from a systematic analysis of the inorganic crystal structure database," Acta Crystallogr. B **41**, 244–247.

Dresselhaus, M. S., Chen, G., Tang, M. Y., Yang, R. G., Lee, H., Wang, D. Z., Ren, Z. F., Fleurial, J. P. and Gogna, P. (**2007**). "New directions for low-dimensional thermoelectric materials," Adv. Mater. **19**, 1043–1053.

Ghamaty, S. and Eisner, N. B. (**1999**). "Development of Quantum Well Thermoelectric films," *Proceedings of the 18th International Conference on Thermoelectrics, Baltimore, MD*, pp. 485–488.

Glazer, A. M. (**1972**). "The classification of tilted octahedra in perovskites," Acta Crystallogr. B **28**, 3384–3392.

Goldschmidt, V. M. (**1926**). "Die Gesetze der Krystallochemie," Naturwissenschaften **14**(21), 477–485.

Grebille, D., Lambert, S., Bourée, F., and Petricek, V. (**2004**). "Contribution of powder diffraction for structure refinements of aperiodic misfit cobalt oxides," J. Appl. Crystallogr. **37**, 823–831.

He, T., Chen, J. Z., Calvarese, T. G., and Subramanian, M. A. (**2006**). "Thermoelectric properties of $La_{1-x}A_xCoO_3$ (A=Pb, Na)," Solid State Sci. **8**(5), 467–469.

Hiramatsu, H., Yanagi, H., Kamiya, T., Ueda, K., Hirano, M., and Hosono, H. (**2008**). "Crystal structure, optoelectronic properties, and electronic structures of layered oxychalcogenides *M*CuO*Ch* (M=Bi, La; *Ch*=S, Se, Te): effects of electronic configurations of M^{3+} ions," Chem. Mater. **20**, 326–334.

Howard, C. J. (**1982**). "The approximation of asymmetric neutron powder diffraction peaks by sums of Guassian," J. Appl. Crystallogr. **15**, 615–620.

Hsu, K. F., Loo, S., Guo, F., Chen, W., Dyck, J. S., Uher, C., Hogan, T., Polychroniadis, E. K., and Kanatzidis, M. G. (**2004**). "Cubic $AgPb_mSbTe_{2+m}$: bulk thermoelectric materials with high figure of merit," Science **303**, 818–821.

Hu, Y. F., Si, W. D., Sutter, E., and Li, Q. (**2005**). "*In-situ* growth of c-axis-oriented $Ca_3Co_4O_9$ thin films on Si(100)," Appl. Phys. Lett. **86**, 082103.

Larson, A. C. and von Dreele, R. B. (**2004**). *General Structure Analysis System (GSAS)* (Report LAUR 86-748). Los Alamos, USA: Los Alamos National Laboratory.

Luu, S. D. N. and Vaquelro, P. (**2013**). "Synthesis, structural characterization and thermoelectric properties of $Bi_{1-x}Pb_xOCuSe$," J. Mater. Chem. A, **1**, 12270–12275.

Masset, A. C., Michel, C., Maignan, A., Hervieu, M., Toulemonde, O., Studer, F., and Raveau, B. (**2000**). "Misfit-layered cobaltite with an anisotropic giant magnetoresistance: $Ca_3Co_4O_9$," Phys. Rev. B **62**, 166–175.

Mikami, H., Itaka, K., Kawaji, H., Wang, Q. J., Koinuma, H., and Lippmaa, M. (**2002**). "Rapid synthesis and characterization of $(Ca_{1-x}Ba_x)_3Co_4O_9$ thin films using combinatorial methods," Appl. Surf. Sci. **197**, 442–447.

Mikami, M. and Funahashi, R. (**2005**). "The effect of element substitution on high-temperature thermoelectric properties of $Ca_3Co_2O_6$ compounds," J. Solid State Chem. **178**, 1670–1674.

Mikami, M., Funahashi, R., Yoshimura, M., Mori, Y., and Sasaki, T. (**2003**). "High-temperature thermoelectric properties of single-crystal $Ca_3Co_2O_6$," J. Appl. Phys. **94**(10), 6579–6582.

Nolas, G. S., Sharp, J., and Goldsmid, H. J. (**2001**). *Thermoelectric: Basic Principles and New Materials Developments* (Springer, New York).

PDF (**2017**). Powder Diffraction File, produced by International Centre for Diffraction Data, 12 Campus Blvd., Newtown Squares, PA, 19073-3273, USA.

Rietveld, H. M. (**1969**). "A profile refinement method for nuclear and magnetic structures," J. Appl. Crystallogr. **2**, 65–71.

Shannon, R. D. (**1976**). "Revised effective ionic radii and systematic studies of interatomic distances in halides and chalcogenides," Acta Crystallogr. A **32**, 751–767.

Shin, W. and Murayama, N. (**2000**). "Thermoelectric properties of (Bi, Pb)-Sr-Co-O oxide," J. Mater. Res. **15**(2), 382.

Terasaki, I., Sasago, Y., Uchinokura, K. (**1997**). "Large thermoelectric power in $NaCo_2O_4$ single crystals," Phys. Rev. B **56**, 12685–12687.

Thompson, P., Cox, D. E., and Hastings, J. B. (**1987**). "Rietveld refinement of Debye-Scherrer synchrotron X-ray data from Al_2O_3," J. Appl. Crystallogr. **20**, 79–83.

Toby, B. H. (**2001**). "*EXPGUI*', a graphical user interface for GSAS," J. Appl. Crystallogr. **34**, 210–213.

Tritt, T. M. (**1996**). "Thermoelectrics run hot and cold," Science **272**, 1276–1277.

Venkatasubramanian, R., Siivola, E., Colpitts, T., and O'Quinn, B. (**2001**). "Growth of one-dimensional Si/SiGe heterostructures by thermal CVD," Nature **413**, 597–602.

Wang, S., Venimadhav, A., Guo, S., Chen, K., Li, Q., Soukiassian, A., Schlom, D. G., Pan, X. Q., Wong-Ng, W., Vaudin, M. D., Cahill, D. G., and Xi, X. X. (**2009**). "Structural and thermoelectric properties of $Bi_2Sr_2Co_2O_y$ thin films on $LaAlO_3$ (100) and fused silica substrates," Appl. Phys. Lett. **94**, 022110.

Wong-Ng, W., McMurdie, H. F., Hubbard, C. R., and Mighell, A. D. (**2001**). "JCPDS-ICDD Research Associateship (cooperative program with NBS/NIST)," J. Res. Natl. Inst. Stand. Technol. **106**(6), 1013–1028.

Wong-Ng, W., Yang, Z., Hu, Y. F., Huang, Q., Lowhorn, N., Otani, M., Kaduk, J. A., Green, M. and Li, Q. (**2002**). "Thermoelectric and structural characterization of $Ba_2Ho(Cu_{3-x}Co_x)O_{6+x}$," J. Appl. Phys. **105**(6), 63706.

Wong-Ng, W., Liu, G., Martin, J., Thomas, E., Lowhorn, N., and Otani, M. (**2010**). "Phase compatibility of the thermoelectric compounds in the Sr-Ca-Co-O system," J. Appl. Phys. **107**, 033508.

Wong-Ng, W., Luo, T., Tang, M., Xie, M., Kaduk, J. A., Huang, Q., Yang, Y., Tang, M. and Tritt, T. (**2011**). "Crystal chemistry and thermoelectric properties of compounds in the Ca-Co-Zn-O system," J. Solid State Chem. **184** (8), 2159.

Wong-Ng, W., Laws, W., and Yan, Y. G. (**2013**). "Phase diagram and crystal chemistry of the La-Ca-Co-O system," Solid State Sci. **17**, 107–110.

Wong-Ng, W., Laws, W., Talley, K. R., Huang, Q., Yan, J., and Kaduk, J. A. (**2014**). "Phase equilibria and crystal chemistry of the CaO-$½Nd_2O_3$-CoO_z system at 885 °C in air," J. Solid State Chem. **215**, 128–134.

Wong-Ng, W., Yan, Y., Kaduk, J. A., and Tang, X. F. (**2016a**). "X-ray powder diffraction reference patterns for $Bi_{1-x}Pb_xOCuSe$," Powder Diffr. **31**(3), 223–228.

Wong-Ng, W., Liu, G., Levin, I., Williamson, I., Ackerman, P., Talley, K. R., Martin, J., AlHamdan, K., Kaduk, J. A., and Li, L. (**2016b**). "X-ray diffraction and density functional theory studies of R_2FeCoO_6 (R=Pr, Nd, Sm, Eu, Gd)," Powder Diffr. **31**(4), 259–266.

Zhao, Y., Weider, D. J., Parise, J. B., and Cox, D. E. (**1993a**). "Thermal expansion and structural distortion of perovskite – data for $NaMgF_3$ perovskite. Part I," Phys. Earth Planet. Inter. **76**, 1–16.

Zhao, Y., Weider, D. J., Parise, J. B., and Cox, D. E. (**1993b**). "Thermal expansion and structural distortion of perovskite – data for $NaMgF_3$ perovskite. Part II," Phys. Earth Planet. Inter. **76**, 17–34.